Feasibility of application of iron zeolites for high-temperature decomposition of N_2O under real conditions of the technology for nitric acid production

Edyta Tabor[a,*], Galina Sádovská[a], Milan Bernauer[a,b], Petr Sazama[a], Jana Nováková[a], Vlastimil Fíla[b], Tomáš Kmječ[c], Jaroslav Kohout[c], Karel Závěta[c], Zdeněk Sobalík[a]

[a] J. Heyrovský Institute of Physical Chemistry of the Czech Academy of Sciences, Dolejškova 2155/3, CZ-182 23 Prague 8, Czech Republic
[b] University of Chemistry and Technology, Prague, Technická 5, CZ-166 28 Praha 6, Czech Republic
[c] Joint Laboratory for Mössbauer Spectroscopy, Faculty of Mathematics and Physics, Charles University, V Holešovičkách 2, CZ -180 00 Prague 8, Czech Republic

A B S T R A C T

The long-term stabilities of a group of iron zeolites with MFI, *BEA, and FER structures and similar Fe/Al ratios were evaluated to assess their performance as catalysts for N_2O decomposition. Conditions relevant for the application of the catalyst at the secondary level for N_2O elimination, i.e., directly after the NH_3 oxidation step of the process of nitric acid production, were investigated. These conditions included reaction temperatures of up to 900 °C and the presence of high concentrations of water vapour, oxygen, and NO. The focus of the study was the comparison of the MFI and *BEA zeolites with the FER-based zeolite, a catalyst established as relatively stable under such conditions. The structural analysis of the individual zeolite frameworks and iron species involved a combination of several methods, and provided insight into the framework modification as well as identification and semiquantitative determination of the individual iron species. In the zeolite catalysts, these iron species were in the form of either isolated Fe(II) and Fe(III)-oxo ions, polynuclear Fe(III)-oxo complexes, or small Fe oxide particles. None of the zeolite structures displayed a high extent of structural collapse of the framework; thus, structural collapse does not explain the observed decrease in activity. An investigation of the kinetics of the N_2O decomposition, both before and after ageing under relevant reaction conditions, proved the dominant role of isolated Fe(II) ions that were accessible to the reacting gas-phase molecules. The kinetic study also identified the differences in the ability of the three zeolites to stabilize the active sites in individual framework types during long-term exposure to challenging reaction conditions. It has been shown that, while the isolated Fe(II) ions were present in adequate concentration for N_2O decomposition activity at the relevant temperature region in all three zeolite-based catalysts, the MFI and *BEA zeolites were not able to effectively stabilize the active iron structure during ageing for over 12 days. In contrast, the FER framework survived a test for over 24 days. The iron species formed in MFI and *BEA zeolites during ageing were mostly large FeO_x species and displayed very low activity that approached the activity of FeO_x clusters supported on SiO_2.

1. Introduction

Nitric acid production represents one of the largest sources of environmentally damaging N_2O [1,2]. Effective decomposition of N_2O formed in HNO_3 production has to be implemented in new units and retrofitting of the existing production plants for this purpose is needed. The standard solution represents decomposition of N_2O in tail gases at relatively low temperature (450 °C). However, more advantageous is to locate the catalyst for N_2O decomposition directly down of ammonia burner. This arrangement of the N_2O elimination process requires a catalyst with adequate activity in the high-temperature regime (between 750 and 930 °C), at a space velocity of about 100 000 h^{-1} and in a gas mixture containing N_2O (between 700 and 2000 ppm) together with 10% NO, 15% H_2O, and 2% O_2 [3,4].

The principal problem of this application is the degradation of the catalytic activity over time, which relates directly to the nature of the active surface of the catalyst and also extends to its textural properties. Despite the outset of the first commercial catalysts, a catalyst for the high temperature (HT) decomposition of N_2O that provides sufficient efficiency and durability still remains a challenge. Reliable assessments

of the potential of proposed alternative catalysts have also been limited by the fact that most of the studies have been done using only model mixtures, i.e., in the absence of other gas-phase components [5–7].

Among the zeolite-based catalysts, which have been evaluated for N_2O decomposition in the absence of other gas-phase components, Fe-FER catalysts have been identified as the most active in the low-temperature region. Their activity was linked to the unique structure of Fe-FER, which contains two collaborating Fe(II) ions located in the β cationic positions (Fe coordinated to four oxygen atoms in 6 membered ring with two Al atoms) of FER [8]. However, in the presence of NO, the superiority of the FER zeolite in comparison with the MFI and *BEA - catalysts was usually less pronounced [9,10]. The catalytic activity of most of the relevant iron zeolite catalysts is well established for temperatures between 300 and 500 °C [2,8,11]. Nevertheless, these data do not represent a reliable indication of the performance, and particularly the long-term stability, of the iron zeolite catalysts in the high-temperature regime. Most of the efficient low-temperature (450 °C) catalysts suffer from a risk of deactivation under more demanding conditions. Deactivation can involve the collapse of the structure and other processes that lead to the formation of less active phases. There have already been several studies comparing the relative stabilities of the iron zeolites, which analyse either the effect of variations in the preparation method [11] or focus on the difference in stabilities of catalysts based on different zeolite morphologies [2]. However, their results were limited to conditions applied in N_2O decomposition in the tail gas of nitric acid production (450 °C). Recently, Fe-FER has been recognized as being both active under the relevant reaction conditions and reasonably stable, surviving exposure to an environment closely mimicking the real reaction conditions of high-temperature decomposition for up to 12 days [12]. It has been shown that the Fe-FER (Si/Al 22) sample still retains enough Fe(II) in β cationic positions to provide efficient decomposition of N_2O, achieving conversion of over 90% at the temperatures below 700 °C and a gas hour space velocity (GHSV) of 350 000 h^{-1}. We proposed that most of the activity in N_2O decomposition is attributable to i) the existence of atomically dispersed iron cations, ii) the presence of NO in the reaction stream, and iii) a small oligomeric Fe_xO_y species existing on the zeolitic support [13,14]. Accordingly, the long-term stability was attributed to the ability of the FER to preserve some amount of these active structures during prolonged exposure. Nevertheless, these results do not predict whether the stability of the catalytic performance of the iron zeolite is a unique feature of the FER structure, or whether it could also be obtained for other structurally similar zeolites. As indicated by Kapteijn [2], albeit by the use of less demanding experimental conditions (427 °C; 50 h), the catalytic activity sequence of N_2O decomposition would be FER > MFI, *BEA. Questions remain about the role of the Si/Al ratio and the time dependence of the noticeable partial deactivation of Fe-

FER during longer exposure, which could provide an indication of the real potential of Fe-FER for application in N_2O decomposition.

The primary objective of this paper is to provide an overview of the long-term stability of the catalytic performance for a group of iron zeolites with various framework types. This overview is supported by the analysis of both the framework structures and iron species, and enables evaluation of the applicability of iron zeolites in the high temperature decomposition of N_2O under conditions representative of those involved in nitric acid production. We aim to show whether the previously obtained results for FER-based catalysts represent an exception or a general trend in the applicability of iron zeolites in the HT-N_2O process. This paper provides a combination of kinetic analysis and structural understanding of the active zeolitic materials, with emphasis on their stability under real conditions of high temperature N_2O decomposition.

2. Experimental

2.1. Catalysts preparation and characterization

The iron zeolite catalysts were prepared by a procedure similar to that used for Fe-FER [8,13,15], which based on ion-exchange of the parent zeolite in the NH_4^+ form using an anhydrous solution of $FeCl_3$ in acetylacetone. 5 g of granulated zeolite FER22, Zeolyst, Si/Al = 22.1, CP914, lot no. 2200; FER9, Zeolyst, Si/Al = 9, ZD05048A; (to distinguish ferrierites sample lower index describing Si/Al ratio was used) MFI; Zeolyst, Si/Al = 8.8, CBV2314; or *BEA, Zeolyst, Si/Al = 12.6, CP814 B was dried for 4 h at 120 °C and then impregnated with a solution of $FeCl_3$ (0.76 g) (purum, ≥97%, Fluka) in acetylacetone (16 g) (p.a., ≥99.5%, LachNer). After 12 h the sample was dried in air and then evacuated for 1 h at 100 °C and for 3 h at 350 °C. Then, after cooling to RT, the sample was washed in distilled water and calcined at two temperatures: 450 °C for 12 h, and 950 °C for 4 h. The samples for Mössbauer spectroscopy measurements were prepared using the same procedure but with isotopically enriched $^{57}FeCl_3$, prepared from ^{57}Fe-enriched iron oxide (> 98% ^{57}Fe enrichment; Isoflex, USA). The ageing procedure, as described in [12], involved the exposure of prepared Fe-zeolites to a gas stream, produced by catalytic oxidation of ammonia by air over a platinum grid, consisting of 2% O_2, 15% H_2O, and 10% NO in N_2 at 800 °C for 12 days. The aged samples were indexed with (12d). A detailed time profile of the changes observed during the ageing of Fe-FER22 was produced by varying the length of the ageing periods: 5 days (5d), 12 days (12d) and 24 days (24d).

Chemical analysis of the prepared catalyst was performed using X-ray fluorescence spectroscopy (ARL 9400 XP, Thermo ARL, Switzerland). The chemical composition of the prepared materials is summarized in Table 1.

Table 1
Composition and structure characteristics of Fe-zeolites.

Sample	Si/Al	Fe/Al	Fe	Fe	Fe(II) [a]	Fe[b]	Fe[c]	Fe(II)[a]/Fe	Co$_{max}$/Al	S$_{BET}$	V$_{micro}$
			(wt.%)	(µmol g^{-1})						(m^2 g^{-1})	(cm^3 g^{-1})
Fe-MFI	12.5	0.27	2.75	340	10	14	0.72	0.03	0.29	315	0.149
Fe-MFI(12d)	12.5	0.27	2.75	340	2.0	2.7	0.40	0.004	0.29	316	0.137
Fe-*BEA	12.6	0.24	1.62	290	24	28	0.22	0.08	0.37	196	0.044
Fe-*BEA(12d)	12.6	0.24	1.62	290	1.0	0.8	0.05	0.002	0.37	132	0.025
Fe-FER22	22.1	0.23	0.90	161	32	37	1.5	0.47	0.21	256	0.117
Fe-FER22(5d)	22.1	0.23	0.90	161	13	18	0.80	0.08	0.21	n.d.	n.d.
Fe-FER22(12d)	22.1	0.23	0.90	161	5.8	4.1	0.55	0.03	0.21	276	0.177
Fe-FER22(24d)	22.1	0.23	0.90	161	2.7	1.8	0.07	0.016	0.21	n.d.	n.d.
Fe-FER9	8.8	0.50	9.0	1620	28	31	2.01	0.017	0.33	217	0.053
Fe-FER9(12d)	8.8	0.50	9.0	1620	4.9	6.5	0.08	0.003	0.33	219	0.069

[a] Calculated from NO adsorption.

[b] Concentration of Fe(II) ions in cationic sites from FTIR spectra of adsorbed d_3-acetonitrile.

[c] Concentration of Lewis sites from FTIR spectra of adsorbed d_3-acetonitrile.

2.2. Structural analysis

The structural analysis was performed using following analysis techniques: XRD, N_2 adsorption, temperature programmed desorption (TPD) with O_2 isotopic exchange, SEM imaging, and UV–Vis-NIR, FTIR, and Mössbauer spectroscopies. Both non-aged and aged catalysts were characterized by XRD (Bruker D8, Bruker AXS, USA). The crystallinity was estimated from the integral area of the three dominant bands of the individual zeolites. The surface area and pore size distribution were assessed by nitrogen adsorption-desorption at 77 K (Micromeritics ASAP 2020). The surface area was estimated by Brunauer-Emmett-Teller theory (BET) and the micropore volume by t-plot method. The values of specific surface area were obtained in the range of relative N_2 pressure (p/p^0) from 0.06 to 0.30, with at least $12°$ of freedom for the fitting procedure. Scanning electron microscopy (SEM) (JEOL JSM-5500LV) was performed for both fresh and aged samples.

The UV–vis–NIR reflectance spectra of hydrated samples were obtained with a spectrometer (Perkin–Elmer Lambda 950) equipped with an integrating sphere for diffuse reflectance measurements. The sphere was coated with Spectralon, which served as a reference. The reflectance was recalculated using the Schuster–Kubelka–Munk function $F(R_\infty) = (1 - R_\infty)^2/2R_\infty$, where R_∞ is the diffuse reflectance from a semi-infinite layer.

Infrared spectra were recorded using an FTIR spectrometer (Nicolet 6700) equipped with a liquid N_2-cooled MCT-B detector. The spectrometer with a heated quartz cell with KBr windows was connected to a vacuum and dosing system. Thin, self-supporting pellets of sample $(8–10 \text{ mg cm}^{-2})$ were placed in the holder, which provided a sample transport from the heating region to the measurement position. FTIR spectra were recorded at RT between 4 000 and 400 cm^{-1}, with a single spectrum consisting of 128 scans at the resolution of 2 cm^{-1}. Before measurement, samples were evacuated (10^{-3} Pa) at 450 °C for 3 h. The obtained IR spectra were normalized to a standard sample thickness of 10 mg cm^{-2}. The quantitative analysis of FTIR spectra of adsorbed d_3-acetonitrile were used for determination of the concentration of Brønsted or Lewis acid sites, and further of Fe(II) cations. The FTIR spectra were collected after d_3-acetonitrile adsorption at pressure of 10 Torr at RT for 30 min followed by evacuation at 200 °C for 30 min. The calculation of the concentration of the individual species was done using extinction coefficients determined previously [13] i.e. $(\varepsilon_{Fe} = 7.12 \text{ cm } \mu\text{mol}^{-1}; \varepsilon_L = 3.62 \text{ cm } \mu\text{mol}^{-1})$. The exposed Fe(II) ion content was determined using NO as a probe molecule [12]. The Fe(II) concentration was calculated from the normalized area of the band at 1 872 cm^{-1}, using an extinction coefficient, ε_{Fe}, of 3.2 cm μmol^{-1}. This quantification was based on data for Fe-FER with low iron content where iron was predominantly located in cationic position as Fe(II) ions [15,16].

TPD was measured for samples exposed in situ to N_2O at 300 °C for either 5 or 40 min. TPD curves were recorded using a Balzers QMG 420 quadrupole mass spectrometer equipped with a secondary electron multiplier detector; m/e ratios were measured in the range 2–60. Prior to interaction with N_2O the samples (100 mg) were evacuated at up to 900 °C in a heated quartz reactor (total reaction volume of 287 mL).

^{57}Fe Mössbauer spectroscopy was used to investigate the structure of the Fe species in the catalysts. The spectra of both the fresh and aged ^{57}Fe-enriched iron zeolites were measured at RT in a home-made apparatus. This apparatus allowed evacuation at high temperature and transport of the measured sample between the heating and the measurement positions. Before the measurement, the sample was evacuated in situ at 450 °C for 3 h. The spectra were deconvoluted into Lorentzian-shaped components using the MossWinn software. The ^{57}Fe Mössbauer spectra of the samples were collected in a transmission geometry using a constant-acceleration spectrometer equipped with a ^{57}Co/Rh source. The weight of the sample was about 100 mg at the circular area of 1 cm diameter. The spectrometer was calibrated using α-Fe foil and the isomer shifts were given with respect to its RT Mössbauer spectrum. The corresponding Mössbauer parameters: isomer shift (IS), quadrupole splitting (QS), and magnetic hyperfine field (B_{hf}) were ascribed to individual iron species in iron ferrierite, based on previously established parameters [12–18].

2.3. Catalytic tests

The catalytic activities of both the fresh and aged catalysts, in the form of grains with dimensions of ~ 0.2–0.4 mm, was measured over a temperature range of 900–200 °C in a quartz U-shaped fixed-bed reactor. To eliminate the effects of sample modification during experiments at higher temperatures, the measurements were performed in a decreasing temperature sequence. The stabilization time for the conversion data was ~ 60 min, therefore the data represent realistic steady state values. The reaction mixture consisted of 1 000 ppm N_2O, 0.5% NO, 2% O_2, and 10% H_2O, with He as a carrier gas, and the total flow rate was 350 $\text{cm}^3 \text{ min}^{-1}$. A setup of several mass-flow controllers (Aalborg) and a water vapour saturator was used to prepare the reaction mixture. A sample volume of 0.06 cm^3 was used, thus the GHSV was 350 000 h^{-1}. In specified experiments, the zeolite samples were diluted by the excess of NaK-FER in the ratio of 1–5 before preparation of the sample grains for catalytic tests to reach a GHSV value ~ 2 500 000 h^{-1}. The analysis of N_2O, N_2, and O_2 at the reactor inlet and outlet was performed using an in-line connected Advanced Optima (ABB) IR analyzer and a Hewlett Packard 6090 gas chromatograph. In the chromatographic analysis, a Hysep column (packed column) was used for the retention and removal of water vapour. An HP-Plot Q column (30 m × 0.53 mm × 40 μm film thickness), a 5A molecular sieve (30 m × 0.53 mm × 25 μm film thickness), and a thermal conductivity detector (TCD) were used to separate N_2O, N_2 and O_2 and monitor of their concentrations. The reproducibility of the N_2O conversion results was ± 2%. The mass balance of the converted N_2O and the produced N_2 and O_2 were proven during the experiment. The influence of external mass and heat transfer on the reaction was excluded by experiments that varied the catalyst weights and flow rates at constant GHSV, in which the conversion of N_2O did not change (within ± 2%). The effect of intra-grain diffusion constraints was evaluated by experiment with catalyst grains whose dimensions were varied from 0.1 to 0.4 mm. The crystal sizes of the parent zeolites were < 1 μm, which guaranteed the absence of intra-crystalline diffusion constraints, as shown in preceding studies for reactions at temperatures below 500 °C.

Kinetic data were modelled as first order reactions with respect to the N_2O partial pressure [19]. The experimental reactor was approximated by an ideal plug flow reactor, and adjustable parameters (activation energy E_a and k_a rate constant) were estimated by weighted nonlinear regression of the experimental data.

3. Results and discussion

3.1. Composition of the samples

A summary of the properties of the iron zeolites, including their Si/Al ratio, acidity, and the exchange capacity of a divalent cation (as revealed by the established technique-based on ion exchange of a Co(II) ion [20]) iron loading, and textural properties is presented in Table 1.

3.2. X-ray diffraction analysis

The XRD patterns of the parent MFI, *BEA, and FER zeolites, and the prepared Fe catalysts both before and after ageing are compared in Fig. 1. The XRD spectra of the parent zeolites show intensities and peaks that are characteristic of the well-developed crystalline structure of MFI, *BEA, and FER topologies. The ageing process results in a decrease in the intensity of the characteristic reflections by $\sim 16, 28, 16$ and 6% for Fe-MFI(12d), Fe-*BEA(12d), Fe-FER$_9$(12d), and Fe-FER$_{22}$(12d), respectively, reflecting a distinct decrease in the degree of crystallinity of
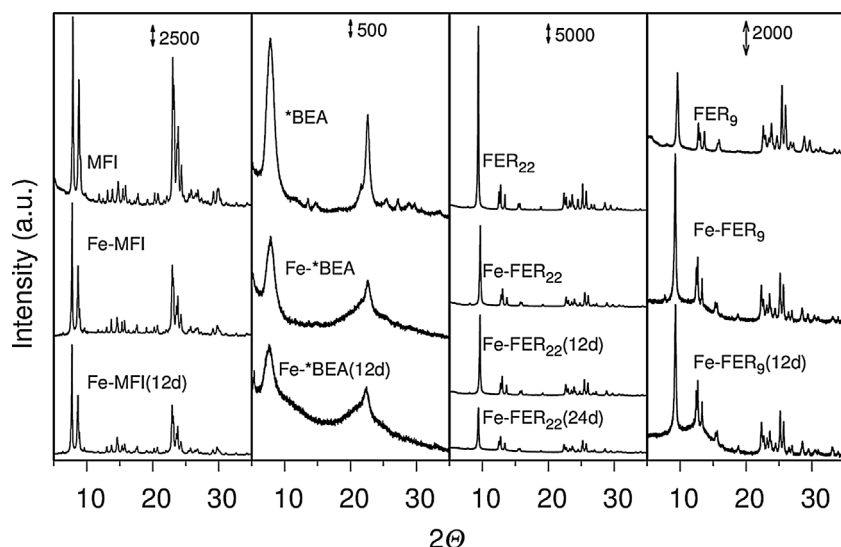
Fig. 1. XRD of non-aged and aged zeolite samples.

the zeolites after ageing. The reflections that remained unchanged correspond to the parts of the zeolite framework that are resistant to the severe thermal and hydrothermal treatments, and maintain their structural order and regular periodic arrangement. The very slight decrease in the crystallinity of Fe-FER$_{22}$ indicates the unique structural stability of the FER structure, which significantly exceeds those of the other zeolites. The absence of reflections corresponding to iron oxides for all the zeolite samples confirms a high dispersion of iron species throughout each sample, within the sensitivity of the XRD method.

The process of the partial destruction of the Fe-*BEA sample during ageing was revealed by the sorption experiments, which showed a decrease in microporosity, as indicated by both the micropores volume (V_{micro} from 0.044 to 0.025 cm^3 g^{-1}) and the BET surface area (from 196 to 132 m^2 g^{-1}). On the other hand, the MFI did not display deep structural destruction, showing a similar resistance to the FER-based catalyst (Table 1).

3.3. UV–vis-NIR analysis

The UV–vis-NIR spectra of the Fe-zeolites before and after ageing are compared in Fig. 2. The spectra of the as-prepared Fe-zeolites are characterized by intense and poorly resolved absorption bands in the UV region at 25 000–50 000 cm^{-1} which reflect O → Fe(III) ligand-to-

metal charge transfer (LMCT) transitions from both the ligand oxygens and oxygen atoms in the zeolite framework. The low-intensity absorption edge in the visible light range at about 18 000 cm^{-1} is specific to Fe oxides [12]. The bands at about 25 000 cm^{-1} were assigned to larger polynuclear Fe-oxo species [21–23] and the absorptions at about 28 000–33 000 cm^{-1} to dinuclear Fe(III)-O$_n$-Fe(III) complexes [22] or polynuclear Fe-oxo complexes without specified nuclearity [23,24]. High-energy absorptions above 33 000 cm^{-1} have been attributed to isolated Fe(III) ions with a frequency reflecting their coordination [29]. Because the extinction coefficients for Fe(III)-oxo LMCT absorptions for various highly dispersed Fe(III)-oxo species are similar [25], and the O → Fe(II) LMCT bands are present only in a spectral range of far UV above 50 000 cm^{-1} [26], the occurrence of the individual bands in the spectra of Fe-zeolites reflects the distribution of the Fe(III)-oxo species. Fe-MFI exhibited a band at 47 000 cm^{-1} corresponding to isolated T$_d$-coordinated Fe(III), an intense bands at ~ 40 000 cm^{-1} reflecting O$_h$-coordinated Fe(III), and a low-intensity below 30 000 cm^{-1} indicating the low content of clustered Fe(III)-oxo species. The spectrum of Fe-*BEA is dominated by a band at 33 000 cm^{-1} corresponding to bridging or polynuclear Fe(III)–oxo complexes. The shoulder at ~ 18 000 cm^{-1} in the spectrum of Fe-*BEA indicates a higher amount of iron oxides compared to Fe-MFI. Fe-FER exhibit low-intensity bands at 40 000 cm^{-1} reflecting isolated O$_h$-coordinated Fe(III)-oxo ions, and a
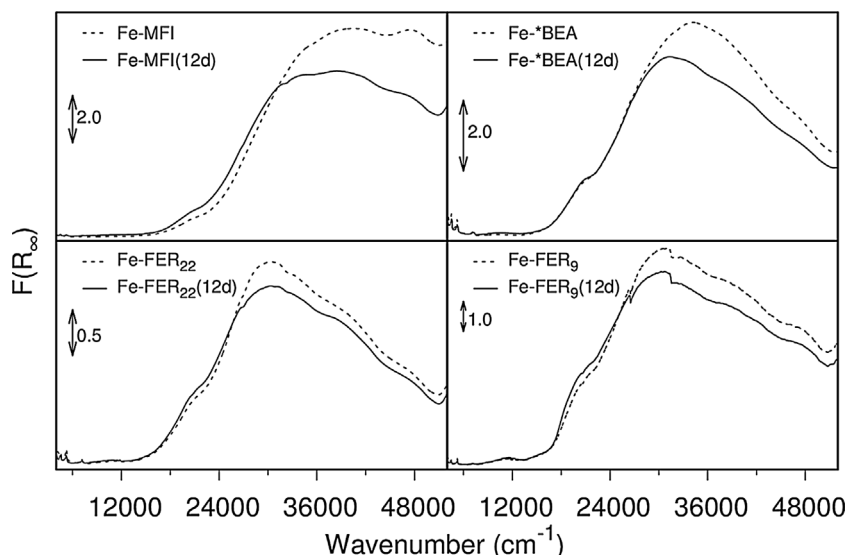
Fig. 2. UV-vis-NIR diffuse reflectance spectra of non-aged (dashed curve) and aged (solid curve) iron zeolites.
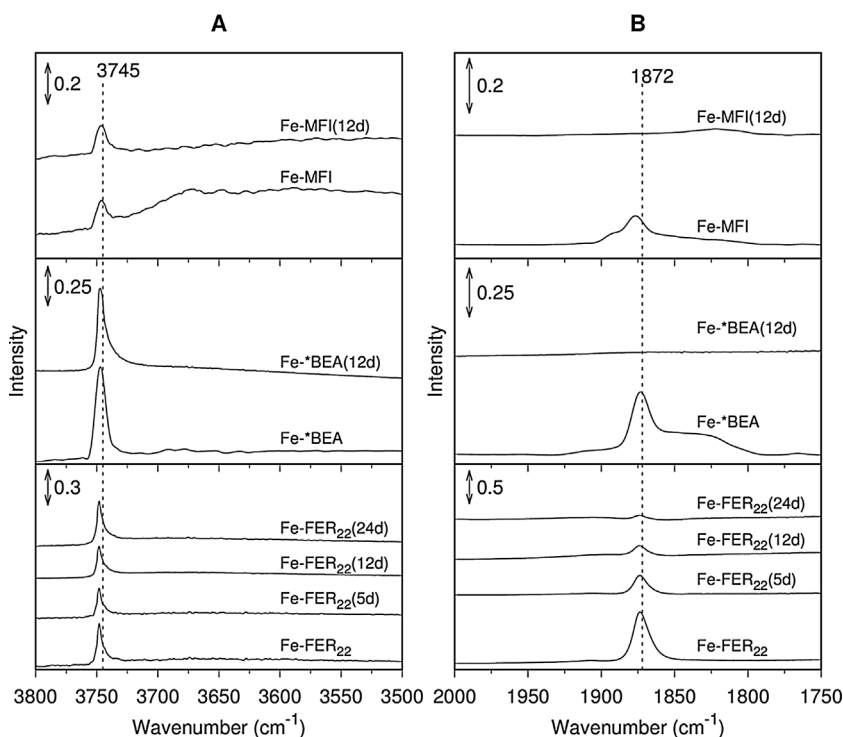
Fig. 3. FTIR spectra of the non-aged and aged iron zeolites after 3 h evacuation at 450 °C region of OH vibrations A) and after interaction with NO (0.7 Torr) region of mononitrosyl vibrations (B).

high intensity at 32 000 cm^{-1} corresponding to bridging or polynuclear Fe(III)–oxo complexes. The band at about 18 000 cm^{-1} indicates the limited amount of iron oxide species likely present on the external surface of zeolite crystals. After ageing of the Fe-zeolites, the intensity of the charge-transfer bands corresponding to isolated Fe(III)-oxo and oligomers at 30 000–50 000 cm^{-1} decreases strongly, indicating the migration of highly dispersed Fe(III) ions, and their agglomeration into Fe oxides is reflected by an increase of the band at 18 000 cm^{-1}.

3.4. FTIR acidity and NO adsorption

The region of OH groups vibrations of the Fe-zeolites evacuated at 450 °C is presented in Fig. 3. Both types of Fe-zeolites before and after ageing exhibited the band at 3745 cm^{-1}, which characterized the terminal silanol groups, which were stable during the ageing treatment. However, in FTIR spectra of both non-aged and aged Fe-zeolites the band at 3603 cm^{-1} typical for Brønsted acid sites, is missing, which indicated complete dehydroxylation of the bridging OH bonds (Fig. 3A).

Analysis of FTIR spectra of Fe-zeolites after d_3-acetonitrile adsorption confirmed the presence of the band at 2311 cm^{-1}, which characterized weakly Al Lewis sites, the intensity of this band dramatically decreased after the ageing (see Table 1). Moreover, after d_3-acetonitrile interaction with non-aged Fe zeolites exhibited a side the band at 2303 cm^{-1} typical for Fe(II)-d_3-acetonitrile complex. Intensity of this band for Fe-MFI and Fe-*BEA was significantly lower than for Fe-ferrierites (Table 1). For all aged Fe-zeolites the concentration of Fe(II) detected by d_3-acetonitrile adsorption was several times lower in comparison with non-aged Fe-zeolites (Table 1). Analysis of FTIR spectra of non-aged and aged Fe zeolites after both dehydration at 450 °C and d_3-acetonitrile interaction showed that the acidity of the zeolites due to Al ions was nearly eliminated (Table 1).

The second method to determine Fe(II) concentration was NO adsorption on non-aged and aged Fe-zeolites. Divalent Fe species present in zeolites formed with NO the mononitrosyl complex visible as band at ∼1872 cm^{-1} (Fig. 3B) [8,26,27]. Both, non-aged Fe-MFI and Fe-*BEA contained lower concentration of Fe(II) in comparison with Fe-FER$_9$ and Fe-FER$_{22}$ zeolites (Table 1). After ageing among studied Fe-zeolites,

only Fe-ferrierites contained the typical Fe(II)-NO complex.(Fig. 3B, and Supplementary Information Figs. S1, S2). Moreover, in the case of Fe-FER$_{22}$ with increasing of the ageing time the decreasing of the intensity of the band characterized Fe-NO is observed (Fig. 3B). The changes in the Fe(II) content in the Fe-FER$_{22}$ depending on the ageing time are also visible in the region of T-O-T vibrations, where the presence of Fe(II) is manifested by the bands at 915 cm^{-1} (β cationic sites) and 926 (α cationic sites) cm^{-1} [14–17]. With prolongation of ageing time of Fe-FER$_{22}$, the decrease of the amount of Fe(II) in β cationic positions was also observed [12] (Supplementary Information Figs. S1, S2). A summary of the semi-quantitative evaluation of the Fe(II) content in the individual samples is given in Table 1.

3.5. TPD results

The aim of the TPD experiments was to evaluate the amount of stabilized surface oxygen atoms during a short exposure of Fe-zeolites to N$_2$O, and to evaluate both the catalysts properties during desorption and their capacity for O$_2$ isotopic exchange [28]. The non-aged iron zeolites (Fig. 4) underwent a short exposure to N$_2$O at a temperature below 300 °C (under conditions where N$_2$O decomposition produces N$_2$ as the only product) and the O$_2$ desorption was monitored. The relative amounts of desorbed O$_2$ strongly decreased for the aged sample. While the exposure of both non-aged and aged Fe-FER$_9$ samples revealed the conversion of surface species into NO$_x$, the formal composition of the species was changed after ageing, showing higher oxidation state of the NO$_x$ surface species over fresh Fe-FER$_9$. The oxygen species formed after a short exposure of the fresh sample to N$_2$O exhibited typical low-temperature isotopic exchange with molecular oxygen (^{18}O$_2$), indicating typical reactivity for the oxygen atoms that were bound to the Fe(II) cations. The reactivity of this oxygen species left on the zeolites was examined using the isotopic exchange for gaseous ^{18}O$_2$ at 50 °C, i. e. at the temperature before the desorption of this oxygen starts. It appeared that about 10% of this oxygen undergoes the exchange on both fresh Fe-FER$_{22}$ and 5 days aged Fe-FER$_{22}$(5d) catalyst. This fraction rapidly increases with increasing temperature to 300 °C, however, it is mixed with the starting ^{16}O$_2$ desorption (Fig. 4). The extent of the isotopic exchanged decreases on Fe- FER$_{22}$(5d) exposed to longer
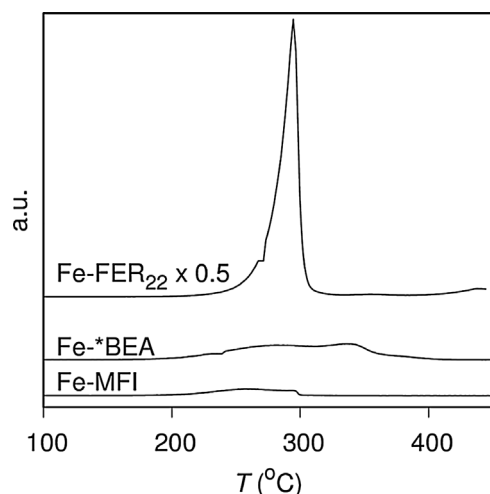
Fig. 4. TPD from non-aged Fe-zeolites after interaction with N_2O at 300 °C.

Table 2
Mössbauer parameters and spectral contribution of fresh and aged: [57]Fe-MFI (~ 1.0 wt.% [57]Fe) and [57]Fe-*BEA (~ 1.0 wt.% [57]Fe) evacuated 3 h at 450 °C.

Zeolite	Component	IS	QS	B_{hf}	Rel.	Fe species
		(mm s^{-1})		(T)	%	
[57]Fe-MFI	D1	0.96	0.56		6	Fe(II)
	D2	0.30	1.46		47	Fe(III)oxo O_h
	D3	0.22	0.95		15	Fe(III) Fe-Al-Si, T_d
	S1	0.38		37	32	Fe(III)-oxo species
[57]Fe-MFI(12d)	D2	0.32	1.46		32	Fe(III)oxo O_h
	D3	0.31	0.84		25	Fe(III) Fe-Al-Si, T_d
	S1	0.38		37	43	Fe_2O_3
[57]Fe-*BEA	D1	0.96	0.48		7	Fe(II)
	D2	0.30	1.38		50	Fe(III)oxo O_h
	D3	0.28	0.98		11	Fe(III) Fe-Al-Si, T_d
	S1	0.38		37	32	Fe(III)-oxo species
[57]Fe-*BEA(12d)	D2	0.32	1.52		30	Fe(III)oxo O_h
	D3	0.21	0.87		29	Fe(III) Fe-Al-Si, T_d
	S1	0.38		37	41	Fe_2O_3

exposure under realistic condition as well as on Fe-*BEA and Fe-MFI zeolites so that it can be hardly evaluated. After short exposures of the Fe-*BEA and Fe-MFI to N_2O oxygen desorption below 300 °C was much lower than for the Fe-FER$_9$ samples. After ageing the desorption of O_2 was observed only for Fe-FER$_9$ (12d) (Supplementary Information Fig. S3).

3.6. Mössbauer spectroscopy

Mössbauer spectra of [57]Fe- MFI and *BEA samples before and after ageing, together with the fitted curves, are presented in Fig. 5 and compared to Fe-FER shown before [13–15,17,18]. Mössbauer spectra were deconvoluted (Table 2) using previously established parameters [14,15] and allowed the characterization of both the Fe(II) located in cationic positions and the Fe(III) species present in the zeolites. The D1 component, which represents the Fe(II) species was observed only in fresh Fe-*BEA and Fe-MFI samples. The concentration of Fe(II) species was 6 and 7% of total iron for Fe-MFI and Fe-*BEA, respectively. The values of Mössbauer parameters characterizing Fe(II) species: IS = 0.96 mm/s and QS = 0.48 or 0.56 mm/s clearly indicate that Fe (II) is located in β cationic position [12–18]. The aged samples contained exclusively trivalent iron species. The D2, D3 and S1 components

were assigned to various types of Fe(III) species that were present in both the fresh and aged Fe-MFI and Fe-*BEA. The D2 component, which indicates the presence of Fe(III)$_{Oh}$-oxo species, was assigned to oligomeric Fe species. The D3 doublet is characteristic of Fe(III) species in a T_d coordination geometry, and the S1 component was assigned to Fe (III)-oxo species or small iron oxide particles. The same trends were seen in the changes in the content of specific Fe(III) species after ageing for both Fe-MFI and Fe-*BEA zeolites. Comparison of the non-aged Fe-MFI and Fe-*BEA with their aged analogues confirmed the increasing concentrations of iron oxide (S1) species (> 40% of total Fe) and Fe(III) species in T_d coordination geometries (Fe-Al-Si; D3) (> 25% of total Fe). The amount of Fe present as O_h oxo species (D2) decreased after ageing, from 47 to 32% and 50 to 30% for Fe-MFI and Fe-*BEA, respectively. Recently presented [12] Mössbauer studies of fresh and aged Fe-FER showed that the concentration of Fe(II) species in Fe-FER decreased after ageing, from 28 to 6%.

3.7. Summary of structural features

The results of X-ray diffraction analysis confirmed that the zeolites structure was preserved after treatment at 950 °C for all non-aged Fe-zeolites (Fe-FER, Fe-*BEA, Fe-FER$_9$ and Fe-FER$_{22}$). Among aged Fe-
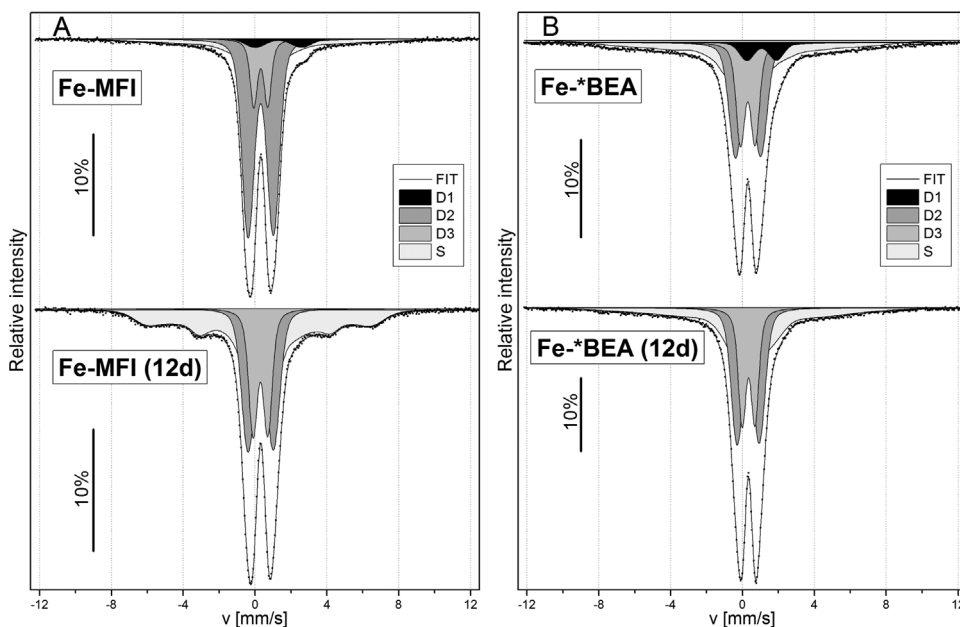

Fig. 5. Mössbauer spectra after 3 h evaluation at 450 °C of non-aged and aged [57]Fe-MFI (A) and Fe-*BEA (B).

zeolites, Fe-ferrierites and Fe-MFI showed a significantly higher structural stability in comparison with Fe-*BEA, where the partial structure collapse was observed (sorption experiments). Comparison of UV–Vis-NIR spectra of non-aged and aged Fe-zeolites confirmed that ageing significantly increased the tendency towards agglomeration of the iron species and iron oxides formation. Presence of Fe(II) species located in β cationic positions in non-aged Fe-zeolites was approved by both FTIR and Mössbauer studies. The highest concentration of Fe(II) in β cationic positions was exhibited by Fe-ferrierites. After the ageing Fe-*BEA and Fe-MFI contained exclusively Fe(III) species. However, aged Fe-ferrierites (with broad Si/Al ratio) kept some part of Fe(II) fraction, it suggests that FER framework offered the special arrangement for Fe(II) species. The framework Al atoms in the studied zeolites showed mostly similar responses during exposure to high temperature, i.e., to calcination at 950 °C in the final step of the catalysts preparation, and during ageing. As in the case of Fe-FER, the acidity of the zeolites was nearly eliminated (Table 1).

3.8. Catalysis and kinetic analysis

The results of catalytic tests performed with both non-aged and aged Fe-zeolites are summarized in Fig. 6, and the calculated results of the kinetic analysis are summarized in Table 3. The non-aged zeolite catalysts showed near-complete conversion of N_2O at temperatures higher than 700 °C and GHSV of 350 000 h^{-1}. The superiority of the Fe-FER over Fe-MFI and Fe-*BEA was clearly performed after the ageing. While the both aged Fe-MFI and Fe-*BEA performed 30% conversion of N_2O (at T > 700 °C) aged Fe-FER operated in these temperatures with 90% N_2O conversion (Fig. 6). A previous study showing the stability of Fe-FER_{22} after 12 days of ageing was extended by increasing the length of the catalyst ageing to 24 days, which showed that increasing the ageing time induces further deactivation, which is accompanied by partial skeletal deterioration.

For catalytic experiments using fresh zeolites and the full reaction mixture, the calculated value of apparent activation energy (E_a calculated for GHSV 350 000 h^{-1}) at high-temperature are nearly identical for both Fe-*BEA (103 kJ mol^{-1}) and Fe-MFI (104 kJ mol^{-1}), suggesting a similar reaction mechanism.

The lower E_a value observed for Fe-FER (90 and 70 kJ mol^{-1} for Si/Al 22 and 9, respectively) could be interpreted as due to the transport limitations playing an important role for Fe-ferrierites, while the structure of Fe centres and their function are similar in all zeolitic structures [11,14,29].

After ageing the E_a of Fe-FER_{22} decreased from 90 to 72, 66, and 59 kJ mol^{-1} for samples aged for 5, 12 and 24 days, respectively. Rate

of N_2O decomposition decreased with prolongation of the ageing time and it correlates with the content of Fe(II) as is presented in Fig. 7. However, the values of E_a for the aged Fe-MFI and Fe-*BEA increased to over 110, 140 kJ mol^{-1}, respectively. The values of E_a for aged Fe-MFI and Fe-*BEA zeolites approach those obtained for SiO_2-based FeO_x catalysts.

3.9. Structure-performance relationship

The structural analysis was based on a combination of several techniques that had already been shown to provide relevant information concerning both the zeolite as well as the iron species. As anticipated, the length of exposure time for which the catalysts were stable to the reaction conditions proved to be decisive for the feasibility of application of these catalysts. When assessing the relevance of the results for the real process, it should be admitted that the validity of the results is limited, even if the experiments used realistic gas stream compositions and temperature regions. On the other hand, the experiments were realized at a space velocity that was ~3 times higher than would be needed for the application of the technology. The difference between the stability of the FER, MFI, and *BEA catalysts during ageing was significant and could not be explained by some of the less-relevant structural effects, including the difference in the Si/Al ratio between the studied catalysts. The Fe-FER based on Si/Al ratios of 22 (see the previous study [12]) and 9 (this study) display similarly high stability. Thus, the difference in the Si/Al ratio of FER (Si/Al, 9, 22), *BEA (Si/Al 12.6), and MFI (Si/Al 12.5) could not satisfactorily explain the stability difference. As anticipated, under long-term exposure to the products of ammonia oxidation at a relevant temperature, all three zeolites underwent near-complete elimination of the aluminium responsible for their Brønsted or Lewis acidity.

When comparing the performance of the non-aged catalysts, during the limited time of the catalytic experiment all three iron zeolites displayed reasonable activity in the high-temperature region under the complete gas stream. Such behaviour correlates with the content of catalytically relevant Fe(II) active species stabilized at structurally specific variants of the β cationic sites in the three zeolites [12–18]. There exists a basic difference between the individual zeolites, as shown by the retention of a small amount of the regularly bonded Fe(II) cations after the long-term treatment by Fe-FER, and their complete absence (or negligible presence) in the Fe-*BEA and Fe-MFI structures. A similar tendency was found by the group of Kapteijn et al. [2], although their experimental conditions were milder. Beside that Fe-FER is structurally more stable than Fe-*BEA and Fe-MFI, the stability of zeolite structure could be not the main reason of the differing resistance of ageing. We propose that these differences can be interpreted by the resistance of the isolated iron species itself against transformation into less active iron oxo species. Accordingly, the relative stability of the local Fe(II) located in β cationic position is proposed to be the decisive parameter controlling the response of the catalytic activity to the ageing [8,13,18,30]. However, the first tentative evaluation of the similar arrangement of divalent cations in the β sites of MFI and *BEA show less symmetric arrangements of the β cationic site occupying divalent cations.

The removal of Al ions from zeolite structures would include those framework Al ions, which do not participate in coordination of Fe(II) in cationic positions. Presence of two Al atoms in 6MRs stabilizes Fe(II) and conversely the iron species protect this site against dealumination. The structure-performance results further support the dominant role of the exposed Fe(II) cations, both before and after exposure to the ageing conditions, in the decomposition of N_2O (Figs. 6 and 7). The complex nature of the transformation of the Fe(II) in the β cationic sites under the conditions of the long-term experiment means there is still lack of relevant theoretical analysis of the stability of the Fe(II) species in high silica zeolites. We recommend a further basic study of the structural conditions for high stabilization of various Fe(II) in high silica zeolites.
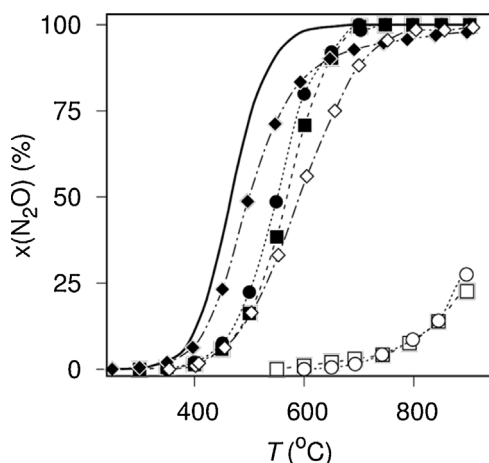

Fig. 6. Catalytic activity of iron zeolites at GHSV of 350 000 h^{-1} in complete gas composition: ■ Fe-MFI, □ Fe-MFI(12d), ● Fe-*BEA, ○ Fe-*BEA(12d), ◆ Fe-FER_9, ◊ Fe-FER_9(12d), ■ Fe-FER_{22} [12].

Table 3
Calculated kinetic parameters: activation energy E_a and apparent reaction rate constant k_A along with calculated N_2O conversion X_{N_2O} and reaction rate R_{N_2O} at T_r.

Sample	X_{N_2O}	k_A (μmol Pa^{-1} g^{-1} s^{-1})	E_a (kJ mol^{-1})	T_{X50} ($°$C)	R_{N_2O} (μmol g^{-1} s^{-1})
GHSV = 350 000 h^{-1} (T_r = 600 °C)					
Fe-MFI	68.8	0.09	104	570	5.2
Fe-MFI(12d)	0.6	4·10^{-4}	110	~1010[b]	0.04
Fe-*BEA	79.7	0.15	103	550	7.7
Fe-*BEA(12d)	0.2	2·10^{-4}	140	960	0.02
Fe-FER$_{22}$	99.8	0.51	90	468	8.2
Fe-FER$_{22}$(5d)	90.6	0.20	72	504	7.9
Fe-FER$_{22}$(12d)	75.5	0.12	66	537	6.5
Fe-FER$_{22}$(24d)	45.0	0.05	59	616	4.0
Fe-FER$_9$	88.2	0.19	70	507	8.1
Fe-FER$_9$(12d)	51.3	0.06	85	597	4.5
GHSV = 2 500 000 h^{-1} (T_r = 800 °C)					
FeFER$_{22}$	41.0	0.30	61	844	23.6
FeFER$_{22}$(5d)	30.0	0.20	61	900	16.6
FeFER$_{22}$(12d)	7.1	0.04	67	~1250[b]	4.0
FeFER$_{22}$(24d)	3.8	0.02	77	~1350[b]	2.0

[b] Extrapolated value.
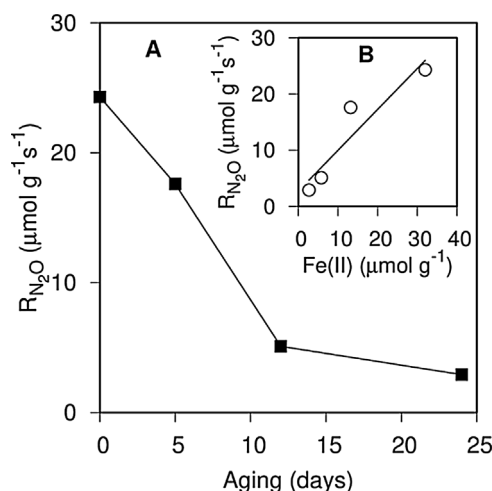
Fig. 7. Rate of N_2O decomposition (800 °C) as function of aging (A) and as function of Fe(II) content (B) of the Fe-FER$_{22}$ at GHSV of 2 500 000 h^{-1}.

By assuming the importance of the ability of a zeolite local structure to stabilize the Fe(II) species that are key to the observed N_2O decomposition activity, our results indicate a clear correlation between the catalytic activity and the local zeolite structure that is preserved in the FER zeolite, but is lacking from zeolites based on the MFI and *BEA frameworks. The exclusivity of the local arrangement of FER in the β site is further highlighted. As shown by our experiments, the decrease in activity of the other studied zeolites is a rather slow process since the fresh catalysts did not show any activity decrease over the course of several hours. By taking into account all of the information obtained in this study, the feasibility of the application of the zeolite-based catalysts for the HT-N_2O decomposition process should not be excluded. Nevertheless, the parameters controlling the long-term stability, including the local properties of the active site relevant for high activity, involve a complex combination of structural features and chemical composition. Only the Fe(II) β structures (Fe(II) coordinated to a local structure with two Al ions and an optimal coordination of the ligand O-atoms) were identified as a candidate structure that preserved high activity during the long exposition to the reaction conditions. Other arrangements were either less stable (including six-member rings in *BEA and MFI, or other iron species typical for iron zeolites- see also [13,14]), or showed only very low activity (e.g., the products of Fe species transformation in MFI and *BEA after ageing).

4. Conclusions

It has been shown that zeolite-based iron catalysts have potential for application in the HT decomposition of N_2O under conditions relevant to those used for nitric acid production. These conditions include temperatures and stream compositions representative of those found downstream of the Pt-Rh wires in NH_3 oxidation. Resistance of the catalysts to the effects of long-term exposure to these demanding conditions is directly connected to the stabilization of the local Fe(II) structure and this structure's resulting resistance to transformation into less active iron oxide species. Until now, such a specific local arrangement with the required stability had been found only in the FER zeolite.

Acknowledgments

Appendix A. Supplementary data

Supplementary data associated with this article can be found, in the online version, at http://dx.doi.org/10.1016/j.apcatb.2017.11.014.

References

[1] J. Pérez-Ramírez, Appl. Catal. B 70 (2007) 31–35.
[2] I. Melian-Cabrera, C. Mentruit, J.A.Z. Pieterse, R.W. van den Brink, G. Mul, F. Kapteijn, J.A. Moulijn, Catal. Commun. 6 (2005) 301–305.
[3] F. Kapteijn, J. Rodriguez Mirasol, J.A. Moulijn, B. Appl Catal, Appl. Catal. B Environ. 9 (1996) 25–64.
[4] P. Esteves, Y. Wu, C. Dujardin, M.K. Dongare, P. Granger, Catal. Today 176 (2011) 453–457.
[5] D.V. Ivanov, L.G. Pinaeva, L.A. Isupova, E.M. Sadovskaya, I.P. Prosvirin, E.Y. Gerasimov, I.S. Yakovleva, Appl. Catal. A 457 (2013) 42–51.
[6] L.G. Pinaeva, L.A. Isupova, I.P. Prosvirin, E.M. Sadovskaya, I.G. Danilova, D.V. Ivanov, E.Y. Gerasimov, Catal. Lett. 143 (2013) 1294–1303.
[7] J. Kruk, K. Stolecki, K. Michalska, M. Konkol, P. Kowalik, Catal. Today 191 (2012) 125–128.
[8] K. Jisa, J. Novakova, M. Schwarze, A. Vondrova, S. Sklenak, Z. Sobalik, J. Catal. 262 (2009) 27–34.
[9] J. Pérez-Ramírez, F. Kapteijn, Catal. Commun. 4 (2003) 333–338.
[10] J. Nováková, Z. Sobalík, Catal. Lett. 111 (2006) 195–202.
[11] G.D. Pirngruber, M. Luechinger, P.K. Roy, A. Cecchetto, P. Smirniotis, J. Catal. 224 (2004) 429–440.
[12] G. Sadovska, E. Tabor, P. Sazama, M. Lhotka, M. Bernauer, Z. Sobalik, Catal.

Commun. 89 (2017) 133–137.

[13] P. Sazama, N.K. Sathu, E. Tabor, B. Wichterlova, S. Sklenak, Z. Sobalik, J. Catal. 299 (2013) 188–203.

[14] P. Sazama, B. Wichterlova, E. Tabor, P. Stastny, N.K. Sathu, Z. Sobalik, J. Dedecek, S. Sklenak, P. Klein, A. Vondrova, J. Catal. 312 (2014) 123–138.

[15] E. Tabor, K. Zaveta, N.K. Sathu, A. Vondrova, P. Sazama, Z. Sobalik, Catal. Today 175 (2011) 238–244.

[16] E. Tabor, K. Jisa, J. Novakova, Z. Bastl, A. Vondrova, K. Zaveta, Z. Sobalik, Microporous Mesoporous Mater. 165 (2013) 40–47.

[17] Z. Sobalik, J. Novakova, J. Dedecek, N.K. Sathu, E. Tabor, P. Sazama, P. Stastny, B. Wichterlova, Microporous Mesoporous Mater. 146 (2011) 172–183.

[18] Z. Sobalik, E. Tabor, J. Novakova, N.K. Sathu, K. Zaveta, J. Catal. 289 (2012) 164–170.

[19] A. Heyden, A. Bell, F. Keil, J. Catal. 233 (2005) 26–35.

[20] J. Dedecek, Z. Sobalik, B. Wichterlova, Catal. Rev. Sci. Eng. 54 (2012) 135–223.

[21] J. Kiwi, N. Denisov, Y. Gak, N. Ovanesyan, P.A. Buffat, E. Suvorova, F. Gostev, A. Titov, O. Sarkisov, P. Albers, V. Nadtochenko, Langmuir 18 (2002) 9054–9066.

[22] L. Capek, V. Kreibich, J. Dedecek, T. Grygar, B. Wichterlova, Z. Sobalik, J.A. Martens, R. Brosius, V. Tokarova, Microporous Mesoporous Mater. 80 (2005) 279–289.

[23] G.D. Pirngruber, P.K. Roy, R. Prins, Phys. Chem. Chem. Phys. 8 (2006) 3939–3950.

[24] S. Bordiga, R. Buzzoni, F. Geobaldo, C. Lamberti, E. Giamello, A. Zecchina, G. Leofanti, G. Petrini, G. Tozzola, G. Vlaic, J. Catal. 158 (1996) 486–501.

[25] S. Brandenberger, O. Krocher, A. Tissler, R. Althoff, Appl. Catal. A 373 (2010) 168–175.

[26] A. Zecchina, M. Rivallan, G. Berlier, C. Lamberti, G. Ricchiardi, Phys. Chem. Chem. Phys 9 (2007) 3483–3499.

[27] G. Berlier, C. Prestipino, M. Rivallan, S. Bordiga, C. Lamberti, A. Zecchina, J. Phys. Chem. B 109 (2005) 22377–22385.

[28] P.C. Andrikopoulos, Z. Sobalik, J. Novakova, P. Sazama, S. Sklenak, ChemPhysChem 14 (2013) 520–531.

[29] P.K. Roy, G.D. Pirngruber, J. Catal 227 (2004) 164–174.

[30] S. Sklenak, P.C. Andrikopoulos, B. Boekfa, B. Jansang, J. Novakova, L. Benco, T. Bucko, J. Hafner, J. Dedecek, Z. Sobalik, J. Catal. 272 (2010) 262–274.